Journal of Applied Electrochemistry (2006)
DOI 10.1007/s10800-006-9201-4

Numerical and experimental study of the effect of gas evolution in electrolytic pickling

N. IPEK[1], N. LIOR[2], M. VYNNYCKY[1,*] and F.H. BARK[1]
[1]*Department of Mechanics, FaxénLaboratoriet, KTH, SE-100 44, Stockholm, Sweden*
[2]*Department of Mechanical Engineering and Applied Mechanics, University of Pennsylvania, Philadelphia, PA, 19104-6315, USA*
*(*author for correspondence, tel.: +46-8-7906770, fax: +46-8-7969850, e-mail: michaelv@mech.kth.se)*

Received 29 September 2003; accepted in revised form 30 June 2006

Key words: corrosion, electrolytic bubble generation, electrolytic pickling, stainless steel

Abstract

As part of a progressive approach to model the electrolytic pickling process, this paper focuses on the important aspect of hydrogen and oxygen gas evolution on the electrodes and on the steel strip being pickled. The system considered consists of type 316 stainless steel pickled in aqueous sodium sulphate, with lead anodes and stainless steel cathodes. The mathematical model is two-dimensional steady-state, and includes the differential equations describing the effect of migration, giving the potential and current fields, and the Tafel kinetic rate expressions for hydrogen and oxygen gas generation. Experiments were conducted to obtain a better understanding of the process and for model validation. Good agreement between the experimental measurements of the global current efficiency and the model predictions was obtained.

Nomenclature

A_a	anode area (m^2)
$A_{a,b}$	anodic area of steel strip (m^2)
$A_{c,b}$	cathodic area of steel strip (m^2)
A_c	cathode area (m^2)
A_{top}	free surface area of the solution (m^2)
a	bubble radius (m)
c_i	concentration of species i (mol m^{-3})
D_i	diffusion coefficient of species i (m^2 s^{-1})
d	half-thickness of the steel strip (mm)
E_{eq,H_2}	equilibrium potential of the hydrogen reaction at the steel strip (V), $E_{eq,H_2} = E^0_{eq,H_2} - \frac{2.303RT}{F}$pH
E_{eq,O_2}	equilibrium potential of the oxygen reaction at the steel strip (V), $E_{eq,O_2} = E^0_{eq,O_2} - \frac{2.303RT}{F}$pH
E^0_{eq,H_2}	standard potential of hydrogen evolution reaction (V)
zE^0_{eq,O_2}	standard potential of oxygen evolution reaction (V)
F	Faraday constant (96485 C mol^{-1})
$f(\gamma)$	hindered velocity function, $f(\gamma) = (1-\gamma)^2$
H	distance between the free electrolyte surface and steel strip surface (mm)
I_{tot}	total computed current (A)
I_b	computed current passing through the steel strip (A)
I_{eff}	current efficiency, defined in Eq. 36
$\mathbf{i}$	current density vector (A m^{-2})
i_b	current density at the steel strip
i_c	current density due to the cathodic reaction (A m^{-2})
$\mathbf{i}_{H_2}$	current density due to the hydrogen reaction (A m^{-2})
$\mathbf{i}_{O_2}$	current density due to the oxygen reaction (A m^{-2})
$i^{(c)}_{0,H_2}$	exchange current density of the hydrogen reaction at cathodes (A m^{-2})
$i^{(a)}_{0,O_2}$	exchange current density of the oxygen reaction at anodes (A m^{-2})
$i^{(b)}_{0,H_2}$	exchange current density of the hydrogen reaction at cathodic strip (A m^{-2})
$i^{(b)}_{0,O_2}$	exchange current density of the oxygen reaction at anodic strip (A m^{-2})
L	length of the anode and cathode electrodes (mm)
L_b	length of the steel strip (mm)
M	molar weight of a species (kg mol^{-1})
M_{H_2}	molar weight of hydrogen (kg mol^{-1})
M_{O_2}	molar weight of oxygen (kg mol^{-1})
$\mathbf{n}$	normal unit vector
N_i	mass flux density vector of species i (mol m^{-3} s^{-1})
R	universal gas constant (8.31 J mol s^{-1})
Re	bubble Reynolds number
Re_{H_2}	hydrogen bubble Reynolds number

Re_{O_2}	oxygen bubble Reynolds number
T	absolute temperature (K)
U	cell voltage (V)
U_{min}	minimum cell voltage (V)
U_S	Stokes terminal rise velocity (m s^{-1})
U_{S,H_2}	Stokes terminal rise velocity for a single hydrogen bubble (m s^{-1})
U_{S,O_2}	Stokes terminal rise velocity for a single oxygen bubble (m s^{-1})
u_i	mobility of species i (m^2 mol J^{-1} s^{-1})
$\dot{V}_{tot}$	total volume flux of gas (m^3 s^{-1})
$\dot{V}_{tot,O_2}$	total volume flux of oxygen gas (m^3 s^{-1})
$\dot{V}_{tot,H_2}$	total volume flux of hydrogen gas (m^3 s^{-1})
$\dot{V}_{top}$	total volume flux of gas at the free electrolyte surface (m^3 s^{-1})
v	average velocity of the electrolyte solution (m s^{-1})
v_{gas}	local volumetric production rate of gas/unit area (m s^{-1})
v_S	vertical relative volume flux density at the electrodes (m s^{-1})
v_{top}	average velocity of gas at the electrolyte solution/air interface (m s^{-1})
We	bubble Weber number
We_{H_2}	hydrogen bubble Weber number
We_{O_2}	oxygen bubble Weber number
z_i	charge number of species i
z_e	number of electrons transferred during a reaction

Greek symbols

$\alpha_{H_2}^{(c)}$	transfer coefficient for the hydrogen reaction at the cathodes
$\alpha_{H_2}^{(b)}$	transfer coefficient for the hydrogen reaction at the cathodic steel strip
$\alpha_{O_2}^{(a)}$	transfer coefficient for the oxygen reaction at the lead anodes
$\alpha_{O_2}^{(b)}$	transfer coefficient for the oxygen reaction at the anodic steel strip
δ	thickness of the anodes and cathodes (mm)
ε	inner anode–anode and cathode–cathode spacing (mm)
Δ_{eb}	electrode-to-strip distance (mm)
Δ_{ie}	inter-electrode distance (mm)
γ	gas fraction of hydrogen and oxygen bubbles
$\eta_{O_2,a}$	anodic surface overpotential at the lead anodes (V)
$\eta_{H_2,c}$	cathodic surface overpotential at the stainless steel cathodes (V)
$\eta_{O_2,b}$	anodic surface overpotential at the anodic section of the steel strip (V)
$\eta_{H_2,b}$	cathodic surface overpotential at the cathodic section of the steel strip (V)
κ_a	conductivity of the anodes (S m^{-1})
κ_b	conductivity of the steel strip (S m^{-1})
κ_c	conductivity of the cathodes (S m^{-1})
κ_e	conductivity of the electrolyte (S m^{-1})
κ_{eff}	effective conductivity of the electrolyte (S m^{-1})
ξ	nondimensional variable, $\xi = \rho_{O_2} M_{H_2} / \rho_{H_2} M_{O_2}$
μ_C	dynamic viscosity of the continuous phase (kg m^{-1} s^{-1})
Φ_a	electric potential of the anodes (V)
Φ_b	electric potential of the steel strip (V)
Φ_c	electric potential of the cathodes (V)
Φ_e	electric potential of the electrolyte (V)
ρ_C	density of the continuous phase (kg m^{-3})
ρ_{H_2}	density of the hydrogen bubbles (kg m^{-3})
ρ_{O_2}	density of the oxygen bubbles (kg m^{-3})
σ_C	surface tension of the continuous phase (N m^{-1})
Ω_b	domain label for the steel strip
Ω_e	domain label for the electrolyte

Subscripts

a	anode
b	steel strip
C	continuous phase
c	cathode
e	electrolyte
H_2	hydrogen bubbles
i	species i
eq	equilibrium value
O_2	oxygen bubbles
S	Stokes terminal velocity

1. Introduction

Pickling is a process widely used to remove surface oxide layers formed during earlier steps of the steel making process. Electrolytic pickling, in which an electric potential is applied to the steel being pickled, allows the use of a relatively harmless neutral aqueous solution of sodium sulphate. This mitigates various negative consequences of the commonly used chemical pickling process, which uses a highly reactive mixture of nitric and hydrofluoric acid. These negative consequences include the formation of NO_x and acid fumes, metal oxides, and hazardous wastes, as well as large losses of un-oxidized metals due to over-pickling, all of which add significant manufacturing costs. In electrolytic pickling the use of acids and the loss of un-oxidized metals are reduced, and the original metal oxides are transformed to easily-removable metal hydroxides [1–4].

The interest in having a better understanding of electrolytic pickling is further motivated by the fact that there is an increasing demand in the steel

industry for higher production rates, as well as lower capital and operating costs; thus, the time to remove the surface oxide layer has to be shortened, and the pickling process has to be made more efficient. For example, the current efficiency of the electrolytic pickling process, where the steel strip to be pickled is indirectly polarized, has been estimated to be only about 30% [5, 6].

Figure 1 shows a schematic of an industrial electrolytic pickling tank, which this paper addresses, through which an aqueous electrolyte is pumped and recirculated. A stainless steel strip with oxidized surfaces moves between electrode groups across which an electric potential is applied. Each group of electrodes is joined by a connector, to which the current is applied. In Figure 1 only the electrical circuit to the electrodes above the steel strip is shown, but a similar circuit is also provided to the electrodes below the steel strip. The electrode potential creates an electric current that flows through the electrolyte and the strip, which acts as a bipolar electrode. In addition to the passage of current through the strip to promote the removal of the oxide layer, electrolysis of water occurs, which generates hydrogen and oxygen gas bubbles on all of the conducting surfaces. Gas evolution is said to consume most of the current supplied for scale removal [5, 7]; in particular, it is claimed that more than half of the current supplied is spent on oxygen gas evolution [8]. Other authors [9–12] claim, without convincing proof however, that gas evolution to some extent improves the pickling process, in that growing bubbles help to peel away the oxide scale. It is also reported [13] that oxygen gas does not take part in the mechanical peeling of the scale.

In a project initiated by the former Avesta Sheffield AB, now Outokumpu Stainless AB in Avesta, Sweden, in collaboration with FaxénLaboratoriet at the Royal Institute of Technology, Stockholm, Ipek et al. [14] developed an analytical model to study the potential and primary current distributions and energy conversion in an electrolytic pickling cell, although ignoring fluid flow, electrochemical reactions, chemical reactions and electrolysis. The present paper extends that model by

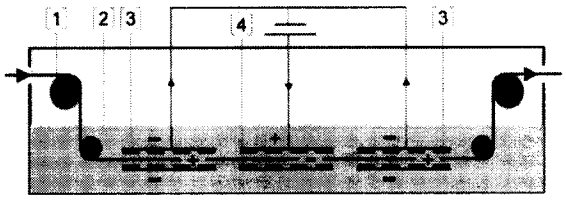

Fig. 1. An industrial electrolytic pickling tank: [1] the steel strip; [2] the electrolyte; [3] the four-cathode set and [4] the four-anode set, both placed symmetrically above and below the moving steel strip. There are four of these electrode assemblies in a typical electrolytic pickling tank.

- including the rate of the reactions, as Tafel laws, that produce oxygen and hydrogen at respective surfaces of the electrode and the bipolar steel strip;
- accounting for the modification of the electrolyte conductivity, due to the production of oxygen and hydrogen bubbles.

In addition, experimental validation is presented. These results are essential components for our ongoing development of a fully coupled electrochemical and hydrodynamic model of the process. The model also allows prediction of the current–potential characteristics as a function of the applied cell voltage and electrode positioning.

The most significant electrochemical reactions occurring in the process, from a fluid mechanical point of view, are those associated with the production of gas bubbles, since their motion creates considerable convection in the electrolyte. Gas evolution on electrode surfaces in industrial processes is reported [15] to have three main fluid dynamical effects: (i) the liquid adjacent to the electrode is periodically replaced; (ii) as the bubbles grow adhering to the electrode surface a micro convective flow is created in their vicinity; (iii) a convective flow is driven by rising bubble swarms. Each of these effects influences the mass transfer in the electrolyte and thus the efficiency of the process. At the same time, the presence of bubbles causes an undesirable increase in the ohmic resistance of the electrolyte [16]. Furthermore, by adhering to, and consequently insulating, a significant part of the electrode and steel strip surfaces, the bubbles cause a non-uniform current distribution. Bubble attachment to the electrode surfaces also increases the overvoltage, due to a significant increase in the actual current density [17]. An experimental cell for a stationary steel strip was built, and electrolytic pickling experiments were conducted to provide insight into the process and to provide data which could be used to support and validate the mathematical modelling. In the electrolytic pickling plant at Outokumpu Stainless AB, the process is run galvanostatically, when treating cold rolled steel strips, typically at current densities of around 0.8–1 kA m^{-2}. Similarly, the experimental set-up was run galvanostatically at 0.1–1.4 kA m^{-2}, in order to study the current efficiency of the process as a function of the applied current density.

Existing models for pickling are restricted to conventional mixed acid pickling [18], where the effect of turbulence on the pickling process was evaluated. No attempt known to us has been made to model the electrolytic pickling process or the gas evolution during the process, although other models do exist that have either taken into account the secondary current distribution in other types of electrochemical cells [19–21] or gas evolution in other types of electrochemical processes [22–26]. We emphasize here, however, that in this paper we do not aim to solve for two-phase flow in combination with the electrochemical conservation equations, as in [22–26]; the aim is rather to derive a

simpler model, in conjunction with experimental measurements.

2. Formulation of the problem

The schematic in Figure 1 is for the Ruthner process and shows one out of four identical electrode assemblies. Each assembly consists of three sets of electrodes in the sequence cathode, anode, cathode; each of these consists, in turn, of four electrodes. As the steel strip passes between the electrode assemblies, it is polarized anodically opposite to the cathodes at the beginning and end of each set, and cathodically opposite to the anode in the centre.

2.1. *Geometry*

The model geometry, illustrated in Figure 2, is based on a cell that was built and used for the pickling experiments. The configuration of the system resembles the electrode configuration in the industrial pickling tank at Outokumpu Stainless AB, although the dimensions are not exactly the same. A typical ratio between the width of the strip in the industrial pickling tank and the strip in our experiment is 20.

The model is a two-dimensional simplification of the experiment to be described in Sect. 4. The third dimension, in the width of the band, was ignored in the model since no differences were observed in the pickled surface of the band in that direction. Due to symmetry only the upper half of the cell is modelled. Here the lead anodes and stainless steel cathodes, of thickness δ and length L and with inter-electrode spacing ε, are at a distance Δ_{eb} from the steel band surface; the shortest distance between the cathodes and the anodes is Δ_{ie}. The steel band has half-width d, length L_b, and conductivity k_b. The rest of the region is filled with an electrolyte of conductivity k_e; the free surface of the electrolyte, through which gas can escape to the surroundings, is at a distance H from the upper surface of the steel band. The aspect ratio of the model geometry, based on the ratio Δ_{ie}/Δ_{eb}, is approximately 12, whereas that in the industrial pickling tank is approximately 22; despite this difference, we believe that the qualitative behaviour of the industrial and laboratory scale processes is nevertheless essentially the same.

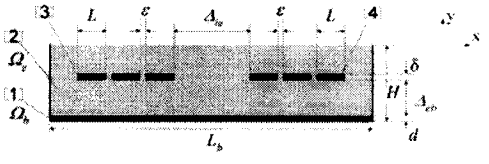

Fig. 2. A cross section of the model geometry showing: [1] the steel strip, [2] the electrolyte; [3] the three-anode set and [4] the three-cathode set. The numerical values for the geometrical parameters, which are the same as in the experiment, are specified in Table 1.

2.2. *Electrochemical reactions*

In this paper we attempt to characterize gas evolution in the electrolytic pickling process, and do not address the electrochemical dissolution reactions of the scale that are reported [5, 6, 9, 13] to take place in the transpassive region of the steel strip at high anodic overpotentials, in parallel with oxygen evolution. Here, simultaneous reactions are regarded as being independent and the net current is taken to be the sum of the different contributions [27]. The pickling reactions are assumed to be decoupled from the gas evolution reactions; this overpredicts, to some extent, the amount of current associated with gas evolution, and thus the gas evolution rates.

The interfacial reaction, at high positive overpotentials, at the anodes and the anodic sections of the steel strip is

$$2H_2O \Leftrightarrow O_2 + 4H^+ + 4e^-, \tag{1}$$

i.e. production of molecular oxygen (released as gas bubbles). Similarly, as a consequence of high negative overpotentials, the interfacial reaction at the cathodes and the cathodic sections of the steel strip is hydrogen gas evolution [2, 6, 28]:

$$2H_2O + 2e^- \Leftrightarrow H_2 + 2OH^-. \tag{2}$$

2.3. *Model equations*

The general expression describing convective, diffusive and migrative transport, N_i, of each ionic species, i, is given by the Nernst–Planck equation [27],

$$N_i = c_i \mathbf{v} - D_i \nabla c_i - \frac{F}{RT} z_i D_i c_i \nabla \Phi_e; \tag{3}$$

however, modifications are required in order to take account of the presence of bubbles within the electrolyte. This is done by introducing the gas volume fraction, γ, a common approach used by Tobias and co-workers [29–31]. In this work, the Bruggeman correlation [32] is used to modify the ionic diffusion coefficients. In summary, the Nernst–Planck equation is then replaced by

$$N_i = c_i \mathbf{v}(1-\gamma) - D_i(1-\gamma)^{3/2} \nabla c_i - \frac{F}{RT} z_i D_i (1-\gamma)^{3/2} c_i \nabla \Phi_e. \tag{4}$$

Here c_i denotes the concentration, D_i the diffusion coefficient, and z_i the charge number of species i. F is Faraday's constant, T is the absolute temperature, $\mathbf{v}$ is the velocity vector of the electrolyte (assumed dilute), and Φ_e is the electric potential field.

The expression for conservation of charge, at steady state, when not accounting for homogeneous chemical reactions in the bulk of the electrolyte, simplifies to

$$\nabla \cdot \mathbf{i} = 0, \tag{5}$$

where

$$\mathbf{i} = F\sum_i z_i \mathbf{N}_i \tag{6}$$

is the current density given by Faraday's law. Assuming a perfectly mixed electrolyte, the diffusive part of Eq. 4 becomes zero. Substituting Eqs. 4 and 6 into 5 and defining the effective conductivity of the electrolyte solution as $\kappa_{\text{eff}} = \kappa_e(1-\gamma)^{3/2}$, where $\kappa_e = (F^2/RT)\sum_i z_i^2 D_i c_i$, and using the electroneutrality condition we arrive at

$$\nabla \cdot \left(-\kappa_e(1-\gamma)^{3/2}\nabla\Phi_e\right) = 0, \quad \text{in} \quad \Omega_e. \tag{7}$$

Here Ω_e is the domain of the electrolyte in the model. In general, γ is a local quantity; here, it will be assumed to be a constant, whose value is to be computed. A technique for obtaining a global estimate for γ will be presented in Sect. 2.5.

As electronic conduction prevails in the bipolar steel strip, Ω_b, there we solve

$$\nabla^2\Phi_b = 0. \tag{8}$$

2.4. *Boundary conditions*

We consider a potentiostatic model, and assume a constant cell voltage, U; without loss of generality, we take the potentials at the anode and cathode electrodes to be $\pm U/2$, respectively.

On the electrode/electrolyte and bipolar steel band/electrolyte interfaces, the normal component of the current density, defining the rate of the electrochemical reactions occurring, becomes, when inserting (4) into (6) and neglecting diffusion,

$$-\kappa_{\text{eff}}\nabla\Phi_e \cdot \mathbf{n} = \mathbf{i}\cdot\mathbf{n}. \tag{9}$$

The normal unit vector, $\mathbf{n}$, here points from the interface into the electrolyte. Since the electrolytic pickling process is operated at high current densities, yielding high positive and negative overpotentials at the respective anode/electrolyte and cathode/electrolyte interfaces, the current density for each of the electrochemical reactions (1) and (2) responsible for gas evolution was approximated by Tafel laws. To account for the reduction of electrode surface area due to blockage by bubbles, we use the approach of Dahlkild [22] and Wedin and Dahlkild [23] and introduce a multiplicative factor $(1-\gamma)$ for the current density.

Combining these ideas, we thus propose the following boundary conditions at the electrodes: at the lead anode, for reaction (1),

$$-\kappa_{\text{eff}}\nabla\Phi_e \cdot \mathbf{n} = i_{0,O_2}(1-\gamma)\exp\left(\frac{\alpha_{O_2}F\eta_{O_2,a}}{RT}\right) \tag{10}$$

and at the stainless steel cathode, for reaction (2),

$$-\kappa_{\text{eff}}\nabla\Phi_e \cdot \mathbf{n} = -i_{0,H_2}(1-\gamma)\exp\left(-\frac{\alpha_{H_2}F\eta_{H_2,c}}{RT}\right). \tag{11}$$

Here i_{0,O_2} and i_{0,H_2} are the respective exchange current densities, α_{O_2} and α_{H_2} the symmetry factors and $\eta_{O_2,a}$ and $\eta_{H_2,c}$ the surface overpotentials, defined as

$$\eta_{O_2,a} = \Phi_a - \Phi_e - E_{\text{eq},O_2}, \quad \eta_{H_2,c} = \Phi_c - \Phi_e - E_{\text{eq},H_2}. \tag{12}$$

In Eq. 12, $\Phi_a = U/2$ and $\Phi_c = -U/2$ are the applied anode and cathode potentials, Φ_e is the potential in the adjacent electrolyte and E_{eq,O_2} and E_{eq,H_2} are the equilibrium potentials for reactions (1) and (2). Since no concentration variations are accounted for, and the electrolyte is assumed neutral, we set pH = 7 everywhere.

The steel strip acts as a bipolar electrode, due to indirect polarization. Therefore, we implement the Tafel rate expressions for oxygen and hydrogen gas evolution at the corresponding anodic and cathodic sections. However, the location of the change in polarization, i.e. surface overpotential, along the steel band is not known beforehand and must be computed as part of the solution. In particular, the normal component of the current density at the steel strip/electrolyte interface is taken as

$$\begin{aligned}-\kappa_{\text{eff}}\nabla\Phi_e \cdot \mathbf{n} = (1-\gamma)\Bigg\{ & i_{0,O_2}\exp\left(\frac{\alpha_{O_2}F}{RT}\eta_{O_2,b}\right)H(\eta_{O_2,b}) \\ & - i_{0,H_2}\exp\left(-\frac{\alpha_{H_2}F}{RT}\eta_{H_2,b}\right)H(\eta_{H_2,b})\Bigg\}\end{aligned} \tag{13}$$

where

$$\eta_{O_2,b} = \Phi_b - \Phi_e - E_{\text{eq},O_2}, \quad \eta_{H_2,b} = \Phi_b - \Phi_e - E_{\text{eq},H_2} \tag{14}$$

and Φ_b is the potential of the steel strip surface. In Eq. 13 we use the Heaviside function H given by

$$H(\Phi) = \begin{cases} 0, & \text{if} \quad \Phi < 0 \\ 1, & \text{otherwise.} \end{cases} \tag{15}$$

Continuity of the normal component of the current density at the steel strip/electrolyte interface gives the boundary condition

$$-\kappa_b\nabla\Phi_b \cdot \mathbf{n} = -\kappa_{\text{eff}}\nabla\Phi_e \cdot \mathbf{n}. \tag{16}$$

At all other boundaries, which are either symmetry planes or insulated, the normal transport rate is zero, so in the absence of transfer of mass and charge we prescribe

$$-\nabla\Phi_b \cdot \mathbf{n} = 0, \quad -\nabla\Phi_e \cdot \mathbf{n} = 0. \tag{17}$$

There are a total of eight kinetic parameters: $i_{0,O_2}^{(a)}$, $\alpha_{O_2}^{(a)}$ and $i_{0,O_2}^{(b)}$, $\alpha_{O_2}^{(b)}$ for the oxygen reaction at the lead anodes and anodic portions of the steel strip; $i_{0,H_2}^{(c)}$, $\alpha_{H_2}^{(c)}$ and $i_{0,H_2}^{(b)}$, $\alpha_{H_2}^{(b)}$ for the hydrogen reaction at the stainless steel cathode and cathodic portions of the steel strip. Values for these parameters were determined from experimental polarization curves and are given in **Table 1**; see [35, 36] for further details concerning the experimental techniques used for obtaining this data.

For homogeneous concentrations, and using a constant value for the gas volume fraction, we require to solve the Laplace equations (7) and (8), subject to the nonlinear kinetics boundary conditions specified by Eqs. 10–19. **Table 1** provides a summary of the data used in the model.

2.5. *Gas volume fraction*

At steady state, the total rate at which gas is produced at the combined surfaces of the electrodes and steel strip should equal the rate at which it escapes from the free surface of the electrolyte. Now, the normal component of the volume flux density at a reaction surface in the dispersed phase is prescribed by the local volumetric production rate of gas per unit area at the electrodes and the strip, v_{gas}, which is determined by the local current density through Faraday's law, i.e.

$$v_{gas} = \frac{(\mathbf{i}\cdot\mathbf{n})M}{z_e F\rho}, \tag{18}$$

where z_e is the number of electrons transferred for the production of each gas molecule, ρ is the density of the gas bubble and M is the molar mass. Integrating over strip and electrode surfaces and summing, we obtain the total volume flux as, $\dot{V}_{tot} = \dot{V}_{tot,O_2} + \dot{V}_{tot,H_2}$, where

$$\dot{V}_{tot,O_2} = \frac{M_{O_2}}{4F\rho_{O_2}}\left(\int_{A_a}(\mathbf{i}_{O_2}\cdot\mathbf{n})dA + \int_{A_{b,a}}(\mathbf{i}_{O_2}\cdot\mathbf{n})dA\right), \tag{19}$$

$$\dot{V}_{tot,H_2} = -\frac{M_{H_2}}{2F\rho_{H_2}}\left(\int_{A_c}(\mathbf{i}_{H_2}\cdot\mathbf{n})dA + \int_{A_{b,c}}(\mathbf{i}_{H_2}\cdot\mathbf{n})dA\right). \tag{20}$$

A_a and A_c denote the areas of the anode and cathode electrodes, respectively, whereas $A_{b,a}$ and $A_{b,c}$ denote the anodic and cathodic sections of the strip. **Table 2** provides a summary of the physical data used for the gas fraction calculations.

To calculate the rate at which gas escapes from the free surface of the electrolyte, we use formulae developed by Wedin and Dahlkild [23], who applied the mixture model formulation for two-phase flow described in [39, 40]. In particular, they presented a number of constitutive laws for the volume-averaged velocity of the mixture based on empirical relations developed for monodisperse suspensions of sedimenting spherical particles. Of most relevance here is the contribution of the vertical relative volume flux density, v_S, directly caused by the buoyancy and given by

$$v_S = \gamma U_S f(\gamma), \tag{21}$$

where U_S is the Stokes terminal rise velocity, given by

$$U_S = \frac{ga^2\rho_C}{3\mu_C}, \tag{22}$$

and $f(\gamma) = (1-\gamma)^2$ is the hindered velocity function [40], which takes into account the fact that the rise velocity of a swarm of bubbles is smaller than that of an individual bubble; other possibilities can also be found in the electrochemical literature [16]. In Eq. 22, a denotes the radius of the bubble, ρ_C the density of the continuous phase (here, the electrolyte), and μ_C its viscosity. These formulae assume that the bubbles remain essentially spherical, which can be justified as long as the bubble Reynolds number, Re, given by

$$Re = 2aU_S\rho_C/\mu_C, \tag{23}$$

Table 1. Base case parameters used in the numerical analysis

δ	3 mm
ε	10 mm
Δ_{eb}	15 mm
Δ_w	15 mm
H	70 mm
d	1 mm
L	20 mm
L_b	300 mm
κ_e [33]	10.18 S m^{-1}
$\kappa_a, \kappa_b, \kappa_c$ [34]	10^7 S m^{-1}
T	298 K
pH	7
$\alpha_{H_2}^{(b)}$, $\alpha_{H_2}^{(c)}$ [35]	0.33, 0.41
$\alpha_{O_2}^{(a)}$, $\alpha_{O_2}^{(b)}$ [35]	0.34, 0.71
$i_{0,H_2}^{(b)}$, $i_{0,H_2}^{(c)}$ [35]	3.2×10^{-3}, 7.9×10^{-4} A m^{-2}
$i_{0,O_2}^{(a)}$, $i_{0,O_2}^{(b)}$ [35]	5×10^{-15}, 5×10^{-10} A m^{-2}
E_{eq,O_2}^0 [28]	1.229 V
E_{eq,H_2}^0 [28]	0 V
E_{eq,O_2} [28]	0.82 V
E_{eq,H_2} [28]	−0.41 V
U	8.65 V

The numbers within the square brackets refer to the list of references.

Table 2. Parameters used in the bubble velocity calculations

$c_{Na_2SO_4}$	170 g l^{-1}
$\mu_{Na_2SO_4}$ [33]	1.51×10^{-3} kg m^{-1} s^{-1}
$\rho_{Na_2SO_4}$ [33]	1133.1 kg m^{-3}
$\sigma_{Na_2SO_4}$ [34]	7.6×10^{-2} N m^{-1}
M_{H_2}, M_{O_2} [34]	2×10^{-3}, 3.2×10^{-2} kg mol^{-1}
ρ_{H_2}, ρ_{O_2} [34]	0.0899, 1.429 kg m^{-3}
μ_{H_2}, μ_{O_2} [34]	8.6×10^{-6}, 2×10^{-5} kg m^{-1} s^{-1}
a_{H_2} [16]	25×10^{-6} m
a_{O_2} [38]	10×10^{-4} m

The numbers within the square brackets refer to the list of references.

is $Re < 1$, i.e. the flow remains within the Stokes regime, and the Weber number,

$$We = 2aU_S^2\rho_C/\sigma_C, \tag{24}$$

is small, typically below 10^{-1}. Here σ_C is the surface tension of the electrolyte.

The rate at which gas escapes through the free surface, $\dot{V}_{top}$, is given by

$$\dot{V}_{top} = \int_{A_{top}} v_{top} dA \tag{25}$$

where A_{top} is the area of the free surface and $v_{top} = v_S/(1-\gamma)$ (see [23]); hence,

$$\dot{V}_{top} = \left(\frac{ga^2\rho_C}{3\mu_C}\right)\frac{\gamma f(\gamma)}{1-\gamma}A_{top}. \tag{26}$$

Setting $\dot{V}_{top} = \dot{V}_{tot}$ and taking into consideration that the total current entering the electrolyte at the anodes equals the total leaving at the cathodes, and the total current entering the steel strip equals the total leaving it, we arrive at

2. The radius of the hydrogen bubbles is taken here as 25 μm [16] and that of the oxygen bubbles as 100 μm [38]. Using Eq. 22, a first estimate of the magnitude of the velocity of a single rising bubble is the Stokes terminal rise velocity, U_S, as

$$U_{S,H_2} = 1.6\times10^{-3}\,m\,s^{-1}, \quad U_{S,O_2} = 2.5\times10^{-2}\,m\,s^{-1}. \tag{31}$$

3. The assumptions used in the model, concerning the Stokes flow and the bubbles' spherical shape, are justified as follows. For hydrogen bubbles, Re_{H_2} is calculated to be of order 10^{-2}, which is within the Stokes flow regime, and the Weber number, We_{H_2}, is of order 10^{-6}. For oxygen bubbles, the Reynolds number, $Re_{O_2} \sim O(1)$ which is only slightly outside the Stokes flow regime, and $We_{O_2} \sim O(10^{-3})$, which is within the model constraints. Thus, the simplified two-phase description given is adequate for both hydrogen and oxygen bubbles.

$$\left(\frac{ga^2\rho_C}{3\mu_C}\right)\frac{\gamma f(\gamma)}{1-\gamma}A_{top} = \frac{(1-\gamma)}{F}\left(\frac{2M_{H_2}}{\rho_{H_2}} + \frac{M_{O_2}}{\rho_{O_2}}\right)\times\left\{i_{0,H_2}^{(c)}\int_{A_c}\exp\left(-\frac{\alpha_{H_2}^{(c)}F}{RT}\eta_{H_2,c}\right)dA + i_{0,H_2}^{(b)}\int_{A_{b,c}}\exp\left(-\frac{\alpha_{H_2}^{(b)}F}{RT}\eta_{H_2,b}\right)dA\right\}. \tag{27}$$

There are several additional caveats concerning the interpretation of Eq. 27:

1. the bubble radius, a, is seen in Table 2 to be four times greater for oxygen than hydrogen bubbles. Which value to use in the calculations depends on which gases have been produced at the strip and the electrodes. Deducing that

$$\frac{\dot{V}_{tot,O_2}}{\dot{V}_{tot,H_2}} = \frac{M_{O_2}}{\rho_{O_2}}\Big/\frac{2M_{H_2}}{\rho_{H_2}} \approx \frac{1}{2}, \tag{28}$$

and taking the terminal rise velocity at the electrolyte surface as a linear combination of the oxygen and hydrogen bubble rise velocities, i.e.

$$U_S = \left(\frac{\dot{V}_{tot,H_2}}{\dot{V}_{tot,O_2}+\dot{V}_{tot,H_2}}\right)U_{S,H_2} + \left(\frac{\dot{V}_{tot,O_2}}{\dot{V}_{tot,O_2}+\dot{V}_{tot,H_2}}\right)U_{S,O_2}, \tag{29}$$

where we weight the velocities according to how much of each gas has been evolved, Eq. 27 yields, on setting $\xi = \rho_{O_2}M_{H_2}/\rho_{H_2}M_{O_2}$,

3. Numerical solution

The problem was solved numerically using the finite element-based PDE simulation code, FEMLAB™ [37]. A grid independence study was made using second-order triangular elements on three different non-uniform meshes, having 17714, 55488 and 181396 cells. The mesh with 55488 cells was used for the calculations, since any further mesh refinement gave only a change in the current density at the surface of the steel band of the order of 0.003%. Furthermore, using an AMD Athlon XP 2000+ (1.667 GHz clock) computer with 2 GB memory, a typical case using 55488 elements took FEMLAB 80 CPU seconds to converge.

In summary, the numerical problem to be solved consists of Eqs. 7 and 8, subject to boundary conditions (10)–(19). This system of equations contains the void fraction γ, which is given implicitly by Eq. 30 and must be iterated for. Thus we solve the problem as follows:

1. Set $\gamma = 0$, and solve Eqs. 7 and 8, subject to boundary conditions (10)–(19).

$$\left(\frac{g\rho_C}{3\mu_C}\right)\left[\left(\frac{2\xi}{1+2\xi}\right)a_{H_2}^2 + \left(\frac{1}{1+2\xi}\right)a_{O_2}^2\right]\gamma f(\gamma)A_{top} = \frac{(1-\gamma)}{4F}\left(\frac{2M_{H_2}}{\rho_{H_2}} + \frac{M_{O_2}}{\rho_{O_2}}\right)\left\{i_{0,H_2}^{(c)}\int_{A_c}\exp\left(-\frac{\alpha_{H_2}^{(c)}F}{RT}\eta_{H_2,c}\right)dA + i_{0,H_2}^{(b)}\int_{A_{b,c}}\exp\left(-\frac{\alpha_{H_2}^{(b)}F}{RT}\eta_{H_2,b}\right)dA\right\}. \tag{30}$$

2. Compute γ using Eq. 30 and return to step (1), this time using the updated value of γ.
3. Re-compute γ and repeat steps (1)–(2) until convergence for is obtained.

The convergence criterion for γ was taken as being when there were no longer any changes in the fourth decimal place; this was usually obtained after 3–4 iterations.

4. Experimental study

The experimental cell and electrode set-up is shown in Figure 3. It consisted of a $360 \times 260 \times 235$ mm^3 rectangular cross-section glass tank [1], containing a neutral solution prepared from pro analysi grade of sodium sulphate 170 g l^{-1}, from Merck and Milli Q water [7], an electrode assembly consisting of two sets of electrodes, with three lead anodes [2], and three stainless steel cathodes [3], placed symmetrically above and below a stationary steel strip, a regulated 9 kW DC power supply, a 1–10 V (± 0.5% + 1 *dgt.*) voltmeter, a 1–10 A (± 1.5% + 1 *dgts.*) ammeter and a 1–400 A clamp-meter. The total area of each electrode assembly was 214 cm^2. There were two magnetic stirrers close to the bottom of the cell (not shown in Figure 3), which could be used to stir the solution, when so desired. The steel strips investigated were of type 316 stainless steel [5], with dimensions $50 \times 3 \times 300$ mm^3, having developed an oxide scale on the surface during the annealing treatment in the annealing and pickling line at Outokumpu Stainless AB. Furthermore, the strip was stationary and supported by two Plexiglas^{TM} holders [4]. To allow measurement of the current passing through the steel strip, it was cut vertically into two equal parts, thereafter two stainless steel rods, type 304SS, Φ4 mm, length 185 mm [6] with a resistance of 0.00012 Ω were screwed on to each half of the strip. The two halves were then glued end-to-end by a 3 mm thick layer of electrically insulating silicon cement; this ensured that the current that passed through the steel strip was forced through the steel rods and the ammeter. The cell was placed onto two magnetic plates for activating the magnetic stirrers when needed. In all experiments, the temperature in the cell was maintained at 24 ± 1/2 °C.

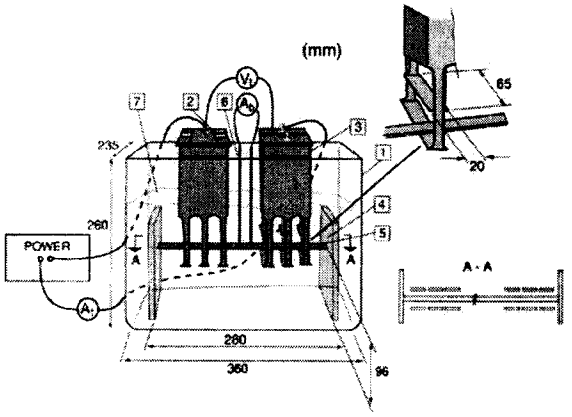

Fig. 3. The experimental cell: [1] the container (glass, $360 \times 260 \times 235$ mm^3); [2] the anodes (lead); [3] the cathodes (stainless steel); [4] the supports (insulating plastic); [5] the steel strip (type 316ss, $50 \times 3 \times 300$ mm^3); [6] the current measurement extension steel rods (type 304ss) and [7] the electrolyte solution (Na_2SO_4). The magnified details in the upper right corner show two views of the electrode-to-strip arrangement and lengths (in mm). The voltmeter (V_t) measures the electrode potential; the clamp meter (A_t) measures the total current and the ammeter (A_b) the current passing through the steel strip.

First, to examine whether cutting the strip as described above would affect the results, an uncut stainless strip was used, the voltage was applied to the pickling cell electrodes, and the corresponding current was measured. It was found that there was no perceptible difference between the current passing in both cases. Experiments were conducted with different inter-electrode distances, Δ_{ie} (the distance between the anode and cathode sets), and electrode-to-strip distances, Δ_{eb}, as illustrated in Table 3, within bounds dictated by the size limitations of the experimental cell. In each of the six cases, the following were held fixed: $H = 70$ mm, $d = 1.5$ mm, $L = 20$ mm, $L_b = 300$ mm, $\delta = 3$ mm, $\varepsilon = 10$ mm. The total current and the current passing through the steel strip were measured for imposed cell voltages in the range 1–13 V.

We also investigated the produced volume of oxygen and hydrogen gas, the sizes of the gas bubbles, and the extent of the influence of the evolving gas on the pickling process. For these purposes, a camera set-up, not shown in Figure 3, was used to photograph the bubble evolution. It consisted of a CCD video camera with magnifying lenses (up to 8 ×), placed in front of the cell. A source of continuous white light (150 W), not shown in Figure 3, was placed on one side of the cell. The images were digitized by the CCD camera, loaded into a Macintosh Power PC by a Scion LG3 frame-grabber card, and analyzed with the NIH Scion Image 1.62 software package. In addition, a DCR-TRV900E CCD camera was used to photograph the pickling process.

5. Results and discussion

We present the results in following order: first, model and experimental results for the base case geometry, where $\Delta_{ie} = 15$ mm and $\Delta_{eb} = 15$ mm; then, the results of the sensitivity study, where Δ_{ie} and Δ_{eb} are varied; and finally, visual observations made in the experiments.

Table 3. Geometrical parameters for the experiments

Case	Δ_{eb}/mm	Δ_{ie}/mm
Ia	15	15
Ib	30	15
IIa	15	65
IIb	30	65

5.1. *Base case geometry*

The geometrical and physical data used in the model, the same as in the experimental cell, are shown in Table 1. As stated earlier, the average current density, referred to the electrodes, used in the industrial pickling plant is around 0.8–1 kA m^{-2}. Consequently we selected a current density of 1 kA m^{-2} for the base case: to obtain this current density in the experimental cell, an applied cell voltage U of 8.65 V was required.

Figure 4(a) illustrates the obtained potential field in the modelled pickling cell for an applied cell voltage, U, of 8.65 V. The cell voltage can be written in terms of its components as

$$U = \sum E_{eq} + U_{ohm} + \eta_{O_2,a} + \eta_{H_2,c} + \eta_{O_2,b} + \eta_{H_2,b}, \quad (32)$$

where $\sum E_{eq}$ is the sum of the equilibrium potentials, i.e. the reversible potential of the system of electrode reactions, U_{ohm} is the ohmic loss in the electrolyte and $\eta_{O_2,a}$, $\eta_{H_2,c}$, $\eta_{O_2,b}$ and $\eta_{H_2,b}$ are the respective overpotentials at the electrode and steel strip surfaces. Here the reversible potentials sum up to about 2.46 V, which implies that about 28% of the applied cell voltage goes to activating the electrochemical reactions in the modelled system. The ohmic losses vary slightly throughout the cell. However, selecting a distance from a point in the electrolyte adjacent to the centre anode/cathode to a corresponding point adjacent to the steel strip surface, the ohmic loss sums up to about 24% of the cell voltage. Note that this model will most likely underestimate the resistance in the cell, and consequently the ohmic loss, because of the use of a global estimate for the gas void fraction. It has, however, been stated [41] that the ohmic losses in the electrolyte are significant in industrial pickling plants due to a large electrode-to-strip spacing, in general about 50–150 mm, and lead to reduced pickling performance. The overpotentials $\eta_{O_2,a}$, $\eta_{H_2,c}$, $\eta_{O_2,b}$ and $\eta_{H_2,b}$ amounts to about 15%, 10%, 11% and 12% of the cell voltage, respectively. This singles out the oxygen evolution reaction as the dominant cause of the voltage drop.

In summary, to increase the efficiency of the pickling cell, one would need to lower either the reversible potential of the system or the ohmic losses by optimising the electrode configuration, which can be done with the aid of computations and Eq. 32. Concerning the overpotential for the oxygen evolution reaction at the lead anodes, the model can convey the benefit of alternative anode materials by introducing experimental kinetic data for the reaction derived for various metals.

The current distribution, Figure 4(b), in the cell reveals that a large fraction of the current passes directly between the anodes and the cathodes without ever entering the steel band, suggesting that the process is not as efficient as it could be. Obviously, the current flows where it encounters least resistance and can be controlled to some extent by optimising the electrode positioning, as is shown in Sect. 5.2.

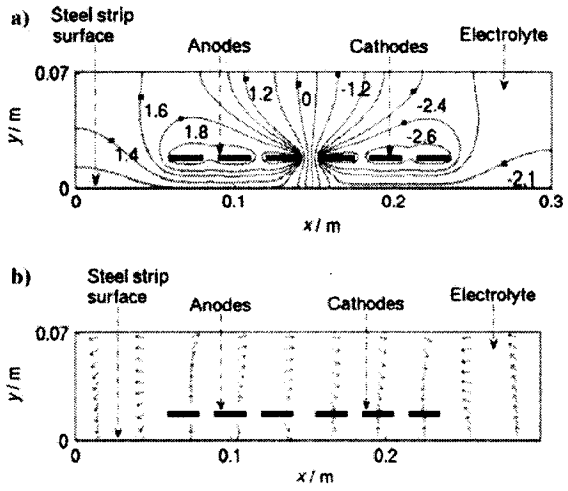

Fig. 4. (a) The potential field (Φ_e) and (b) the current density vector ($-\kappa_{eff}\nabla\Phi_e$) in the electrolyte as calculated from the numerical model, with the base case parameters the same as in the experiments, specified in Table 1. The arrows are normalised and represent only the current direction.

Figure 5 shows the potential difference, $\Phi_b - \Phi_e$, and the current density distribution along the steel strip surface. In Figure 5(a), the bipolar nature of the steel strip is seen: in particular, the strip surface shifts from being cathodically polarized, in the half-cell where the anodes are situated, to being anodically polarized in the half-cell where the cathodes are situated. For this calculation, the global void fraction γ was computed to be 2.5%. The figure also compares the overpotential that would have been obtained had gas evolution not been taken into account, i.e. by setting $\gamma = 0$ the two curves, perhaps somewhat surprisingly, are found to lie on top of each other, a feature we will return to later. In addition, note that the predicted magnitude of the potential difference, shown in Figure 5(a), compares quantitatively with that measured on a steel strip surface in an industrial plant, i.e. about 2 V vs the standard hydrogen electrode (SHE) [9] at the anodic section and −1.8 V vs SHE at the cathodic section (in 15% Na_2SO_4 at 80 °C and an average current density of 500 A m^{-2}) for a steel strip having similar composition to type 316 and travelling with a speed of 0.1 m s^{-1}. The fact that the potential difference measures in the plant is higher than that predicted by our model, although at lower average current density and a significantly higher temperature than in our case, could partly be attributed to the combined effect of lower conductivity and the presence of gas bubbles at the electrode surfaces. This is known to increase the local overpotential, due to induced resistance. The effect of temperature and solution concentration also needs to be further addressed.

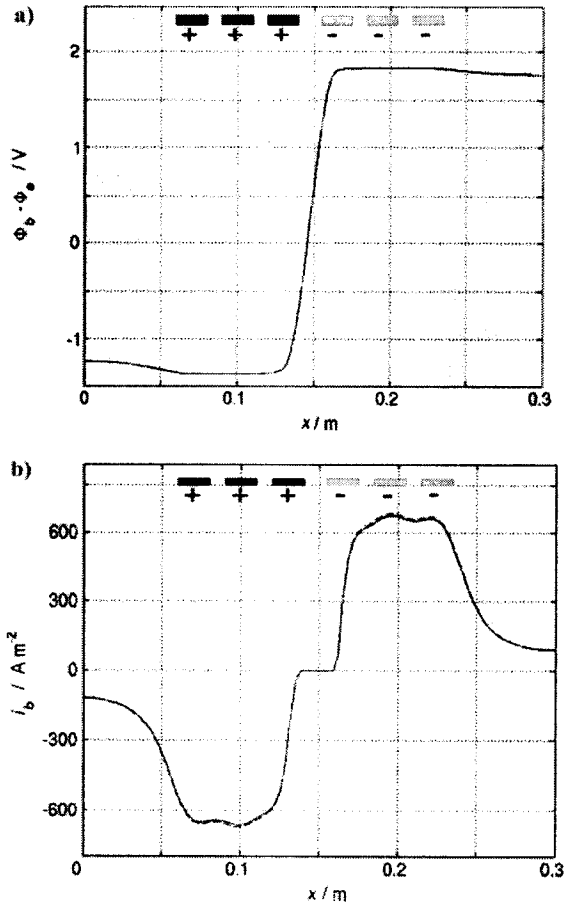

Fig. 5. (a) The potential difference, $\Phi_b - \Phi_e$, and (b) the current density, i_b, at the surface of the steel strip, computed using the base case parameters given in Table 1. The unbroken line is for the case where the gas evolution model is implemented; the dotted line is for the case where gas evolution is neglected.

The form of the potential difference distribution on the steel strip surface, with a slight increase in magnitude below the electrodes, is reflected in the current density distribution along the strip surface, shown in Figure 5(b): there is a local maximum at the strip surface located beneath the middle electrode of cathode set, and a local minimum beneath the middle electrode of the anode set. The relative difference in current density amounts to about 85% between the local maximum and the value of the current density at the end of the anodic strip section. The oxide scale removal was confirmed in our pickling experiments [42] to follow the behaviour of the predicted current density distribution, with a maximum in scale removal under the centre of the cathode set. In addition, the current density was also compared with the results obtained by setting $\gamma = 0$. Here, in contrast to Figure 5(a), a difference between the two is evident; at most this is around 4% at the surface beneath the middle electrode of each electrode set. This illustrates that a global estimate of the gas void fraction does not impose a significant resistance in the pickling cell.

The effect of taking into account the gas void fraction is further illustrated in Figure 6, where current–potential curves with and without consideration of gas evolution are compared. In this figure, the curves denoted by I_{tot} represent the total current passing from the anode to the cathode, whilst I_b denotes the current passing through the steel strip; formally, these are given by

$$I_{tot} = \int_{A_a} (\mathbf{i}_{O_2} \cdot \mathbf{n}) dA, \quad I_b = \int_{A_{b,a}} (\mathbf{i}_{O_2} \cdot \mathbf{n}) dA. \tag{33}$$

From around 9 V and upwards, there are the first signs that the two-phase model ($\gamma \neq 0$) starts to predict lower currents than the single-phase model.

A further interesting observation here is that for cell voltages, U, below 6 V the experimental measurements indicate no significant current passing through the steel strip, although a fluctuating current of magnitude 0.01–0.05 A was measured in the experiment from about 3.5 V. A similar voltage threshold, at about 6 V, is also observed in the computed data, even though here the influence of the oxide scale was not taken into account. The threshold voltage can partly be explained as follows. As was outlined in Eq. 32, a minimum voltage of the same magnitude as $\sum E_{eq}$ in the system, 2.46 V, is needed to activate the electrochemical reactions at the electrode and strip surfaces in the pickling cell. Apart from the sum of the equilibrium potentials, depending on the path of the current, ohmic losses in the electrolyte, surface blockage of the electrodes by generated gas bubbles, and reaction kinetics will increase the resistance in the cell, and put constraints on the attainable current for a specific cell voltage. In conclusion, the observed threshold voltage, at 6 V, is a measure of the voltage needed to overcome the resis-

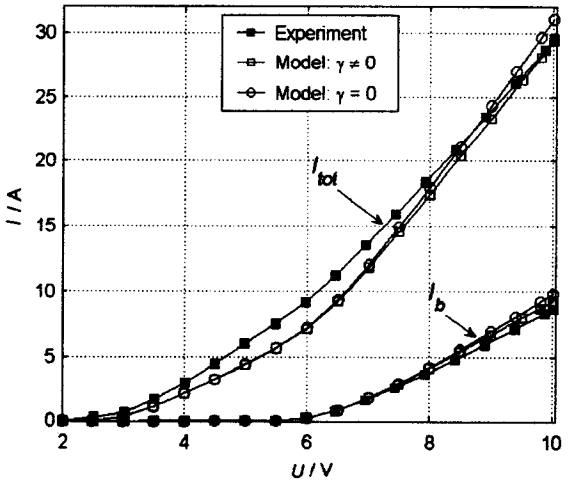

Fig. 6. Comparison of the measured and computed current–potential curves for the whole cell and steel strip for the base case geometry. The numerical data is specified in Table 1.

tance in the pickling cell and conduct a stable current through the strip and of the increased resistance imposed on the steel surface by the oxide scale.

As is also seen in Figure 6, there is a discrepancy between the experimental and calculated values for I_{tot} and I_b. The use of the Tafel approximations, the omission of the oxide dissolution reactions, as well as the simplified boundary condition, Eq. 15, on the steel strip surface, are all possible sources for discrepancy between the experimental and calculated data. It can also be seen that the 2D model does not capture the exact current/potential performance of a 3D experiment: all the more so, since the width of the strip used was less than that of the upper and lower electrodes.

5.2. *Experimental and numerical sensitivity study of the electrode spacing*

Experiments were conducted to determine the effects of electrode spacings, i.e. electrode-to-strip Δ_{eb} and inter-electrode Δ_{ie}, on the current efficiency, I_{eff}, defined as the ratio between the net current passing into the steel strip to the total current passing from the anodes to the cathodes, i.e.

$$I_{eff} := \frac{I_b}{I_{tot}}. \tag{34}$$

Displayed in Figures 7 and 8 are both the measured and computed sensitivities of the current efficiency, I_{eff}, to and Δ_{eb} for different cell voltages, U. General observations from these figures are that current efficiency increases with increasing cell voltage, and with decreasing Δ_{eb}, or increasing Δ_{ie}. The influence of and Δ_{eb} can roughly be summed up as follows (at a cell voltage of 10 V): the relative decrease in the current efficiency, I_{eff}, due to a twofold increase in Δ_{eb} from 15 to 30 mm, was found to be about 40% for Δ_{ie} = 15 mm, and about 30% for Δ_{ie} = 65 mm (for comparison, see Figure 7).

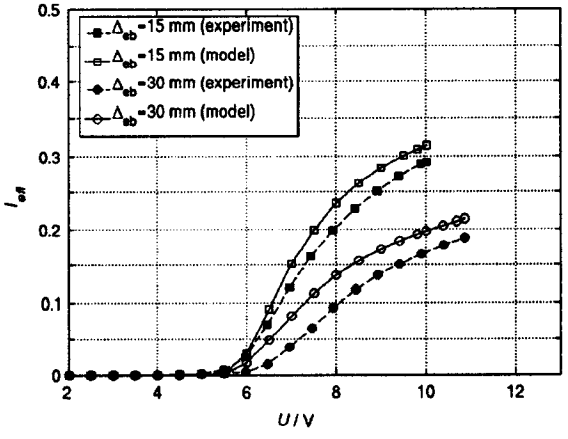

Fig. 7. Comparison of the measured and computed current efficiency, I_{eff}, vs. U for Δ_{ie} = 15 mm. The other parameters used in the simulation are specified in Table 1.

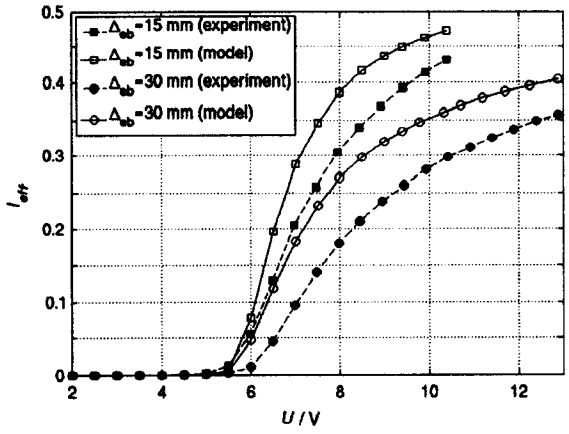

Fig. 8. Comparison of the measured and computed current efficiency, I_{eff}, vs. U for Δ_{ie} = 65 mm. The other parameters used in the simulation are specified in Table 1.

In addition, investigating the effect of Δ_{eb} we observed a relative increase in I_{eff} of about 40% when Δ_{ie} was increased from 15 to 65 mm at Δ_{eb} = 15 mm, see Figure 8. This effect became more pronounced when Δ_{eb} was increased to 30 mm. In conclusion, the mentioned figures will of course differ for varying cell voltages, but the trend will be similar; consequently I_{eff} is seen to be inversely proportional to Δ_{eb} and directly proportional to Δ_{ie}.

The current efficiency predicted by the model is always greater than that based on experimental data. In all cases, I_{eff} only starts to exceed 5% for cell voltages greater than 7 V. Ultimately, it should be kept in mind that I_{eff} is only an indirect measure of the actual pickling efficiency, i.e. the fraction of current that is used for oxide dissolution. Recent work by Ipek et al. [43] showed that, at an anodically polarized steel band surface (cold rolled Type 316), about 7–12% of the applied current was used for oxide dissolution, whilst the remaining part was consumed in the evolution of oxygen gas. At a cathodically polarized steel surface, on the other hand, the hydrogen evolution reaction consumes all the current. Furthermore, the percentages given depend on, among other things, the applied current density and the specific steel grade. Also, the use of a global gas void fraction probably underestimates the effect of the gas evolving reactions on the behaviour of the system. Local gas void fractions can be expected to be much higher than the couple of per cent given here, especially on downward-facing surfaces. It is evident, from Figure 7 for example, that the effect of gas void fraction is most visible where the local current density is highest; thus, we can expect that the modelled current density at the anode and cathode electrodes would be most modified, as compared the single-phase model. Experimentally, it is possible to measure the global gas void fraction by comparing the height of the surface of the electrolyte before and during the experiment; typically, this was found to be around 2%, which

is of the same order of magnitude as given by the computations.

Finally, although the model at this stage is fairly simple and there are clearly numerous sources for discrepancy with the experimental results, the trends are, on the whole, encouraging.

5.3. *Visualization experiments*

As a first approach, we have used geometrical symmetry, both in our experimental configuration and our model. However, in view of the generation of bubbles, it is natural to expect some asymmetry, and we complement the modelling with an experimental study of this; further details are given in [42].

Figure 9 shows a bottom view of two cathodes (Figure 9(a)) and a side-view close up one cathode (Figure 9(b)) producing hydrogen gas during pickling, as well as a bottom view of the steel strip (Figure 9(c)), demonstrating that bubbles coalesce and adhere to the lower surface of the strip. Note the significant difference in size between the bubbles sticking to the bottom surface of the cathode in Figure 9(b) and those escaping from the top surface. Both Figure 9(a) and (c) shows that the bottom surfaces of the electrodes and steel strip become covered by a layer of gas bubbles.

Visual estimates from photographs showed that the bubble coverage on the bottom electrodes and steel strip surfaces, about 20% compares roughly with the 20% coverage reported on Pt-electrodes in stagnant 1 M H_2SO_4 at 1 kA m^{-2} [44], and 30% coverage reported on stainless steel cathodes in stagnant 1 M KOH and 0.1 kA m^{-2} [45]. It is nonetheless known that the bubble coverage in stagnant electrolytes is strongly affected by the current density, material and surface conditions of the electrodes.

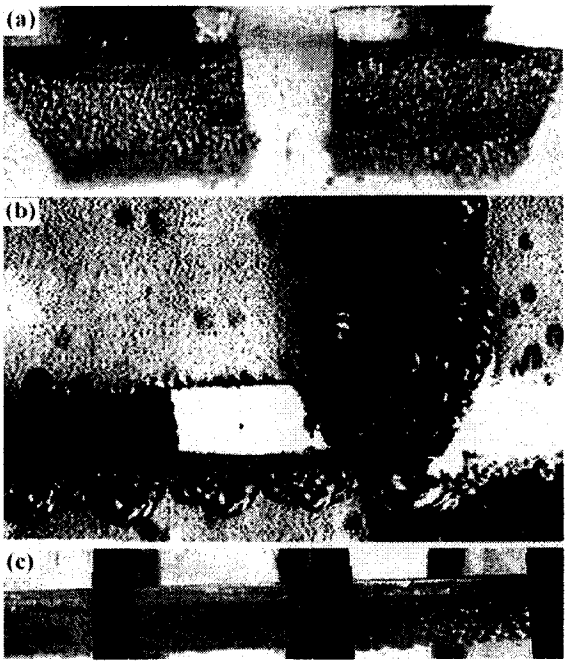

Fig. 9. Photographs of the pickling process taken with a CCD camera at 8 × magnification: 3 min after the start of the pickling experiment in Na_2SO_4. $c_{Na_2SO_4} = 170\ g\ l^{-1}$, and with $\Delta_{eb} = 19$ mm, $\Delta_{ie} = 50$ mm, $U = 6.67$ V, $I = 1.43$ A and $T = 294$ K. (a) View from below of the cathodes. (b) Side view close up of a cathode. (c) View from below of the cathodic polarized section of the steel strip.

The mean diameter of the hydrogen bubbles was estimated by visual inspection in our experiments to be around 130 μm, whilst that for oxygen bubbles was roughly 390 μm. In general, the size of the generated bubbles is known to depend on the electrode material, type of electrolyte and the current density. In the literature [16], the mean diameter of hydrogen bubbles is reported to be 50 μm, with a maximum value of 200 μm. The mean diameter of hydrogen bubbles evolved on stainless steel electrodes was reported [46] to be about 60 μm, at a current density of 0.5 kA m^{-2}. For oxygen bubbles in stagnant alkaline solution on vertical electrodes, the average radius was found to be 24–101 μm [38], whereas on horizontal electrodes, it was found to be slightly larger at 86–138 μm. The mean diameter of the hydrogen bubbles estimated from our experiment and that found in the literature [16] is therefore of the same order of magnitude. However, the mean diameter of the oxygen bubbles was about three times larger; this could be due to coalescence, since we could not measure the size of the bubbles at the actual electrode surface. In view of the tentative nature of our data, we chose for our model to use the earlier and more reliable literature data.

As mentioned earlier, the experiment was conducted both with stationary and stirred electrolyte in order to examine the effects of stirring on the nature of the process and its efficiency. Pickling in stationary electrolyte yielded a compact layer of gas bubbles in the regions immediately above and below the electrodes and steel strip [47]. Hardly any bubbles were dispersed in the electrolyte in the bottom of the cell. Stirring of the electrolyte disperses the bubbles more or less homogeneously throughout the electrolyte, although the stirring rate used did not affect the cell current. It is worth noting that, even in an electrolyte which is not stirred by external means, there is flow due to the bubble rise, coalescence, and bubble collisions. It is reported [45] for horizontal electrodes that the surface coverage of bubbles at flow velocities of 0.02–0.3 m s^{-1} drops from 30% to 2%, when compared with the coverage in stationary electrolyte. This is noteworthy since the ohmic inter-electrode resistance, mass transfer to and from the electrodes and the surface overpotential are affected by the presence of bubbles. In stagnant electrolytes, free convection induced by bubbles was reported [45] to control mass transfer at low current densities, whereas in moving electrolytes, forced convection was stated to interfere with the micro convective mass transfer, due a reduction in the bubble coverage at the surfaces.

6. Conclusions

This paper focused on hydrogen and oxygen gas evolution on the electrodes and on the steel strip in the electrolytic pickling process. A model that takes into account transport due to migration, conservation of charge and incorporates a global estimate of the gas volume fraction, as well as its effect on solution conductivity, was developed. Tafel laws for the gas evolution reactions were also derived with kinetic data obtained from polarization experiments. Small scale pickling experiments were performed using a stationary oxidized steel strip of type 316 in neutral sodium sulphate at room temperature. The main results were as follows:

- good qualitative agreement between experimental measurements and model predictions;
- a predicted nonuniform current density distribution along the steel strip surface which has a maximum whose location agrees well with that of the most pickled area on an experimentally pickled strip;
- the current efficiency varied from effectively zero to 45%, depending on the applied voltage/current density, as well as on the positioning of the electrodes. This encompasses the 30% value for the global process efficiency reported in the literature;
- bubbles were observed to cover about 20% of the electrode and strip surfaces, with significant coalescence on the downward-facing surfaces.

Acknowledgements

Advice from Dr. Anders Eklund at Outokumpu Stainless AB, Professor Göran Lindbergh and Dr. Ann Cornell at the Applied Electrochemistry Department, KTH, and Dr. Arne Nordmark and Dr. Anders Dahlkild at the Department of Mechanics, KTH, and the partial financial support of Outokumpu Stainless AB and VINNOVA, are gratefully acknowledged.

References

1. Anon., Sheet Metal Industries **56** (1979) 36.
2. E. Braun, *Iron Steel Eng.* **57** (1980) 79.
3. B.S. Covino Jr, US Dept. of the Interior, Bureau of Mines (1988) p. 39.
4. R.M. Hudson, ASM International, ASM Handbook: Surface Engineering, Vol. 5 (USA, 1994) 67.
5. V.I. Dunaevskii, V.T. Stepanenko, M.A. Shnyl and L.N. Bespalko, *Protect Met.* **21** (1985) 359.
6. D. Henriet, Surface treatments for stainless steel state of the art development and trends, Final report, EUR 17248 EN. Office for Official Publications of the European Communities, Luxembourg (1996)329 pp.
7. K. Tano, T. Murase, A. Maruta, S. Abe, T. Okazaki and S. Kido, Development of new pickling process for stainless steel sheets (BT-P Process), Nippon Steel Technical Report No. 43 (1989).
8. Y. Kawabata, S. Owada, S. Satoh, F. Togashi, O. Hashimoto, S. Kakihara and T. Kawasaki, Development of electrolytic descaling method for stainless steels using HNO3-HCl acid, Conference Processes and Materials: Innovation Stainless Steel, Florence, Italy, 11–14 October (1993) pp. 2.83–2.87.
9. E.T. Shapovalov, A.P. Shlyamnev, E.A. Ulyanin, V.D. Nikitin, A.R. Fisher, D.B. Goldzon, L.V. Popova and I.I. Milovanov, *Steel USSR* **12** (1982) 215.
10. E.T. Shapovalov and A.P. Shlyamnev, Identification of contactless bipolar pickling mechanism of chromium nickel steels in neutral sodium sulphate solution, International Conference 21st Century Steel Industry of Russia and CIS, Moscow, 6–10 June (1994), pp. 59–60.
11. H. Hugdahl, *Wire J. Int.* **18** (1985) 62.
12. M. Ito, M. Yoshioka, Y. Seino, M. Suzuki, M. Sakuta, Y. Maki and Y. Kawabata, *ISIJ Int. (Japan)* **37** (1997) 391.
13. V.I. Ignat'ev, N.N. Sergeeva and M.A. Shluger, *J. Appl. Chem. USSR* **60** (1987) 258.
14. N. Ipek, N. Lior, F.H. Bark, A. Eklund and A. Alemany, *Russian J. Electrochem.* **38** (2002) 238.
15. H. Vogt, Gas-evolving electrodes, *in* E. Yeager, B.E. Bockris, B.E. Conway and S. Sarangapani (eds), Comprehensive Treatise of Electrochemistry 6, (Plenum, New York, 1983), pp. 445.
16. H. Vogt, *J. Appl. Electrochem.* **13** (1983) 87.
17. F. Hine and K. Murakami, *J. Electrochem. Soc.* **128** (1981) 2314.
18. A.G. Doernemann, *Iron Steel Eng.* **74** (1997) 47.
19. F. Brichau, J. Deconinck and F. Balanck, *Aluminium* **68** (1992) 587.
20. J. Zoric and A. Solheim, *J. Appl. Electrochem.* **30** (2000) 787.
21. R. Akolkar, U. Landau, H. Kuo and Y.-M. Wang, *J. Appl. Electrochem.* **34** (2004) 807.
22. A.A. Dahlkild, *J. Fluid Mech.* **428** (2001) 249.
23. R. Wedin and A.A. Dahlkild, *Ind. Eng. Chem. Res.* **40** (2001) 5228.
24. M.D. Mat, K. Aldas and O.J. Ilegbusi, *Int. J. Hydrogen Energy* **29** (2004) 1015.
25. K. Aldas, *Appl. Math. Comp.* **154** (2004) 507.
26. M.D. Mat and K. Aldas, *Int. J. Hydrogen Energy* **30** (2005) 411.
27. B. Frisch, W. Thiele and E. Scholtes, *Stahl. Eisen.* **110** (1990) 63.
28. J.S. Newman and K.E. Thomas-Alyea, *Electrochemical Systems* (John Wiley & Sons, New Jersey, 2004), pp. 647.
29. R.E. DeLa Rue and C.W. Tobias, *J. Electrochem. Soc.* **106** (1959) 827.
30. C.W. Tobias, *J. Electrochem. Soc.* **106** (1959) 833.
31. R.E. Meredith and C.W. Tobias, *J. Electrochem. Soc.* **110** (1963) 1257.
32. D.A.G. Bruggeman, *Annalen der Physik, ser. 5* **24** (1935) 636.
33. V.M.M. Lobo and J.L. Quaresma, *Handbook of Electrolyte Solutions, Part B* (Elsevier, Amsterdam, 1989).
34. Handbook of Chemistry and Physics, 67th edn. 1986–1987, (CRC Press Inc. Boca Raton, Florida).
35. N. Ipek, A. Cornell, M. Vynnycky, A mathematical model for the neutral electrolytic pickling process. I. Single-phase flow (in preparation).
36. A. Cornell, B. Håkansson and G. Lindbergh, *J. Electrochem. Soc.* **150** (2003) D6.
37. Femlab 3.1, http://www.comsol.com.
38. L.J.J. Jansen, C.W.M.P. Sillen, E. Barendrecht and S.J.D. van Stralen, *Electrochim. Acta* **29** (1984) 633.
39. M. Ishii, *Thermo-Fluid Dynamic Theory of Two-Phase Flow* (Eyrolles, Paris, 1975), pp. 248.
40. M. Ishii and N. Zuber, *AIChE J.* **25** (1979) 843.
41. W. Karner, J. Starcevic, US patent No.: 6,120,671 (2000).
42. N. Ipek, N. Lior and A. Eklund, *Ironmaking Steelmaking* **32** (2005) 87.
43. N. Ipek, B. Holm, R. Pettersson, G. Runnsjö and M. Karlsson, *Mater. Corros.* **56** (2005) 521.
44. H. Vogt, *Electrochim. Acta* **25** (1980) 527.
45. J. Eigeldinger and H. Vogt, *Electrochim. Acta* **45** (2000) 4449.
46. P. Boissonneau and P. Byrne, *J. Appl. Electrochem.* **30** (2000) 767.
47. N. Ipek, Mathematical modelling and experimental studies of the electrolytic pickling of stainless steel, Dissertation, Royal Institute of Technology, Stockholm (2006).